

TRACING THE METAL-POOR M31 STELLAR HALO WITH BLUE HORIZONTAL BRANCH STARS

BENJAMIN F. WILLIAMS¹, JULIANNE J. DALCANTON¹, ERIC F. BELL², KAROLINE M. GILBERT³,
PURAGRA GUHATHAKURTA⁴, CLAIRE DORMAN⁴, TOD R. LAUER⁵, ANIL C. SETH⁶, JASON S.
KALIRAI³, PHILIP ROSENFELD⁷, LEO GIRARDI⁸
Draft version June 5, 2022

ABSTRACT

We have analyzed new HST/ACS and HST/WFC3 imaging in F475W and F814W of two previously-unobserved fields along the M31 minor axis to confirm our previous constraints on the shape of M31's inner stellar halo. Both of these new datasets reach a depth of at least F814W<27 and clearly detect the blue horizontal branch (BHB) of the field as a distinct feature of the color-magnitude diagram. We measure the density of BHB stars and the ratio of BHB to red giant branch stars in each field using identical techniques to our previous work. We find excellent agreement with our previous measurement of a power-law for the 2-D projected surface density with an index of $2.6^{+0.3}_{-0.2}$ outside of 3 kpc, which flattens to $\alpha < 1.2$ inside of 3 kpc. Our findings confirm our previous suggestion that the field BHB stars in M31 are part of the halo population. However, the total halo profile is now known to differ from this BHB profile, which suggests that we have isolated the metal-poor component. This component appears to have an unbroken power-law profile from 3–150 kpc but accounts for only about half of the total halo stellar mass. Discrepancies between the BHB density profile and other measurements of the inner halo are therefore likely due to the different profile of the metal-rich halo component, which is not only steeper than the profile of the metal-poor component, but also has a larger core radius. These profile differences also help to explain the large ratio of BHB/RGB stars in our observations.

Subject headings: galaxies: individual (M31) — galaxies: stellar populations — galaxies: evolution

1. INTRODUCTION

Stellar halos of massive galaxies are likely formed in great part from the disruption of dwarf galaxies. The stellar content of these halos thus offer quantitative insight into galaxy assembly (e.g., Bullock et al. 2001; Bullock & Johnston 2005; Bell et al. 2008; Johnston et al. 2008; Zolotov et al. 2009; Cooper et al. 2010; Deason et al. 2013; Pillepich et al. 2014). One key observable property that is typically compared to simulations is the radial stellar density profile. These profiles are commonly measured in nearby galaxies, such as the MW (Jurić et al. 2008; Sesar et al. 2011), M31 (Guhathakurta et al. 2005; Courteau et al. 2011; Ibata et al. 2014), N253 (Bailin et al. 2011; Greggio et al. 2014) and M81 (Barker et al. 2009). However, such profiles have proven difficult to measure over wide radial ranges. In particular, the profile shape of the inner parts ($\lesssim 10$ kpc) of stellar halos are difficult to probe. This shape is important to determine as the density profile at large radii can diverge if extrapolated to zero radius.

Much work has gone into measuring the stellar density profile of M31. M31 makes an excellent case study because it is very nearby, and its halo has been resolved to 150 kpc

(e.g., Ibata et al. 2001; Kalirai et al. 2006a; Gilbert et al. 2007; McConnachie et al. 2009; Gilbert et al. 2009; Courteau et al. 2011; Gilbert et al. 2012; Williams et al. 2012; Dorman et al. 2013; Ibata et al. 2014; Gilbert et al. 2014). Recently, the Panchromatic Hubble Andromeda Treasury (PHAT Dalcanton et al. 2012) has started a new era in the study of M31 by producing homogeneous HST imaging of about 1/3 of the star forming disk. One of the unexpected discoveries from this project was the detection of field BHB stars within M31 bulge fields. The surface density of these BHB stars was found to follow the trend from the outer halo, strongly suggesting that these stars belong to the halo population and allow us to directly measure the inner halo stellar density profile in M31 to previously-unattainable radii (Williams et al. 2012).

Our work with the PHAT data suggested that, if the BHB is indeed a pure halo population, then the stellar halo has a surface density profile with a 2-D power-law index of $\alpha = 2.6^{+0.3}_{-0.2}$ that flattens to $\alpha < 1.2$ in the inner 3 kpc (Williams et al. 2012), and the BHB/RGB ratio of the halo component is relatively constant with radius. These findings about the BHB population of M31 produced predictions of the BHB stars that would be observed

¹ Department of Astronomy, Box 351580, University of Washington, Seattle, WA 98195; ben@astro.washington.edu; jd@astro.washington.edu; philrose@astro.washington.edu

² Department of Astronomy, University of Michigan, 550 Church St., Ann Arbor MI 48109; ericbell@umich.edu

³ Space Telescope Science Institute; kgilbert@stsci.edu; jkalirai@stsci.edu

⁴ UC Santa Cruz; raja@uco.lick.org

⁵ NOAO; lauer@noao.edu

⁶ University of Utah; aseth@astro.utah.edu

⁷ Department of Physics and Astronomy G. Galilei, University of Padova, Vicolo dell'Osservatorio 3, I-35122 Padova, Italy; philip.rosenfeld@unipd.it

⁸ Osservatorio Astronomico di Padova – INAF, Vicolo dell'Osservatorio 5, I-35122 Padova, Italy; leo.girardi@oapd.inaf.it

in previously-unobserved HST fields. If confirmed, these would show that the power law continues to be steep to radii of ~ 3 kpc and turns over to > -1.2 at < 3 kpc, the only measurement of a halo profile to very small radii.

At the same time, there were a number of outstanding questions left open by the BHB stellar halo measurement. The interpretation of these BHB stars traced the halo component hinged on the assertion of a constant BHB/RGB ratio in the halo from 20 kpc (where it was measured in halo only fields) to the inner parts. Since the metallicity of the stellar halo is known to vary with radius, this assertion left open the possibility that inferences of the density profile of the inner stellar halo based on BHB stars were incomplete.

Furthermore, recently there have been several relevant and comprehensive studies of the M31 halo structure by Dorman et al. (2013), Ibata et al. (2014), and Gilbert et al. (2014). Dorman et al. (2013) decomposed the structure of M31 by simultaneously fitting surface brightness, stellar luminosity function, and stellar velocity data. They found a halo profile with a power-law index of 2.5 ± 0.2 , very close to that measured using the BHB stars alone. However, they found a core radius, where the halo stellar profile flattens, to be ~ 10 kpc, apparently at odds with the BHB stars, which clearly continue to follow the ~ 2.5 power-law index well inside of 6 kpc. Confirming previous measurements of a metallicity gradient in the M31 halo (Kalirai et al. 2006b; Koch et al. 2008; Tanaka et al. 2010), Ibata et al. (2014) found that the different metallicity components of the M31 halo have significantly different profiles outside of 27 kpc, so that measuring the metal-poor component, as we trace with the BHB, does not necessarily tell the whole story. Gilbert et al. (2014) quantified the metallicity gradient of the halo with spectroscopically-confirmed members and included radii as small as 9 kpc.

In this paper, we probe BHB stars at intermediate radii, making it possible to test for departures from a $R^{-2.6}$ power law suggested by the outer fields and the inner fields under the assumption that the BHB belongs to the halo component. We find that the BHB projected number density matches a $R^{-2.6}$ profile to within the measurement uncertainties at these radii as well, strengthening the interpretation of the innermost BHB stars as probes of the metal-poor halo at small radii. This result combined with earlier measurements of the stellar halo density at large radii (Gilbert et al. 2012; Ibata et al. 2014), yield a measurement of the metal-poor M31 stellar halo as an unbroken power-law with a 2-D index of ~ 2.6 over a very large radial range (3–150 kpc). Furthermore, the results suggest that the difference in the shapes of the metal-poor and metal-rich halo populations consists of different core radii as well as different power-law indexes. In section 2 we describe our new data and provide a brief reminder of the analysis technique. Section 3 discusses the results and comparison with predictions from previous work, and section 4 provides our conclusions. Throughout the paper, we assume a distance to M31 of 780 kpc (Stanek & Garnavich 1998), and a position angle of the major axis of 38° (Carignan et al. 2006).

2. DATA

We observed the minor axis of M31 with HST for 2 orbits, using the ACS as the primary camera and WFC3/UVIS as the parallel camera on 28 November 2013. The telescope was oriented with $PA_{V3}=259$ degrees, which allowed both the ACS and UVIS fields to fall on the minor axis simultaneously. The footprints of the 2 fields are shown in Figure 1. Each camera obtained one orbit of data in F475W and one orbit in F814W.

Image calibration was performed by the MAST reduction pipeline (OPUS version 2013_2) to produce the processed fit images on which we performed our photometry. The data were put through the same photometry pipeline as that used for the PHAT photometry in Williams et al. (2012), making the reduction identical to that of our previous study. Briefly, the fit images are put through multidrizzle to identify cosmic rays; then they are multiplied by the pixel area map and bad pixels and cosmic rays are masked to prepare the images for photometry. Finally the images are put through the DOLPHOT (Dolphin 2000) point spread function fitting routine to find and measure magnitudes for all of the stars in the image. DOLPHOT outputs quality metrics such as signal to noise sharpness and crowding, which are used to cull the results of artifacts and bad measurements.

After this procedure 236561 and 61657 stars had been measured in the ACS and UVIS fields, respectively, with signal-to-noise > 4 , sharpness² < 0.2 , and crowding < 2.25 in both bands. These quality metrics are discussed in detail in Dalcanton et al. (2012). The resulting color-magnitude diagrams are shown in Figure 2, where the smaller area of the UVIS camera as well as its slightly larger galactocentric distance cause the lower number of stars in the UVIS CMD. The BHB is clearly visible in both CMDs; however, the smaller number of BHB stars in the UVIS CMDs does result in somewhat larger uncertainties, especially in the fraction of BHB to RGB stars.

Once the photometry was complete, we determined the number of BHB and RGB stars using the same method as Williams et al. (2012). In short, the number of BHB stars is measured by first fitting the F814W luminosity function in the color range $0.1 < F475W - F814W < 0.5$ with the sum of a line and a Gaussian (see Figure 3). Once fitted, the integral of the line alone (non-BHB stars) is subtracted from the integral of the fitted function to obtain the number of BHB stars. The number of RGB stars was measured by counting the number of stars in a box of CMD space where $22.0 < F814W < 22.5$ and $1.5 < F475W - F814W < 3.5$.

3. RESULTS AND DISCUSSION

We have placed the measured BHB star densities and BHB/RGB fractions from our two new fields on the same plots as Williams et al. (2012) in Figures 4 and 5. The lines on the plots are not fits with the new data, but the same lines used in the previous analysis. These lines correspond to the halo profiles measured by Williams et al. (2012), Courteau et al. (2011), Guhathakurta et al. (2005), and Dorman et al. (2013). The new observations are consistent with the fits to the data from Williams et al. (2012) while probing a previously-unobserved radius. The fact that the density falloff mimics the expected drop from the inner radii to the outer radii shows that the BHB component of these

fields are not strongly affected by substructure.

More importantly, the earlier data showed a steep transition at these radii from low BHB/RGB ratio at the inner radii, where the RGB was highly contaminated by disk and bulge stars, to a relatively constant ratio of 0.7. The previous measurements resulted in a prediction of a smooth increase in BHB/RGB ratio at these radii to the constant 0.7 value. Indeed, the new observations confirm that the ratio follows the predicted smooth transition; however, new studies have since been published on the metallicity properties of the halo with radius. In light of these studies, the interpretation of this transition is more complicated.

Given that the BHB stars are tracing the metal-poor stellar halo, it is difficult to reconcile the fact that their density distribution clearly follows a continuous power-law to galactocentric distances inside of 6 kpc while sophisticated decompositions based on a much larger amount of data suggest that the stellar halo density distribution flattens outside of 8 kpc (Courteau et al. 2011; Dorman et al. 2013).

Since our technique uses BHB stars, it necessarily only probes the metal-poor component of the stellar halo, suggesting that this component has a smaller core than the total stellar halo. Over the past decade, M31’s halo has been shown to have a metallicity gradient (Kalirai et al. 2006b; Koch et al. 2008; Tanaka et al. 2010). Recently, Ibata et al. (2014) found that the “unmasked⁹” projected stellar density profile of the outer halo of M31 is a strong function of metallicity, with the more metal-rich component ($[\text{Fe}/\text{H}] > -1.1$) having a steep fall-off ($\alpha \sim 3.7$) at large radii. Their lower metallicity profiles ($[\text{Fe}/\text{H}] < -1.1$) have similar slopes to the BHB stars ($2.3 < \alpha < 2.7$). Thus it is possible that the discrepancy between the BHB results and the kinematic and surface brightness results for the inner regions is attributable to the metal-rich and metal-poor components of the stellar halo having different profiles. This possibility affects the use of the BHB in understanding both the mass and profile of the M31 stellar halo.

Below we explore the possibility that the explanation for the discrepancy between the multiple profile measurements is metallicity. Herein, we simplify the problem by breaking the halo into 2 components: one metal-rich and one metal-poor. M31’s halo is likely more complex than this simple two-component model—the distribution of metallicities is present in the population with radius is a mixture of stars with a range of metallicities. However, the BHB are likely to mainly represent the metal-poor populations in the halo. As shown below, the large core radius measured by Dorman et al. (2013) and the small core radius measured using the BHB stars can be somewhat reconciled if (1) the observed differences between the profiles of the metal-rich and metal-poor stars persist into the inner regions of the halo, and (2) the large core radius measured by Dorman et al. is comprised primarily of metal-rich halo stars.

3.1. The Stellar Halo Profile

Recent work confirms that the power-law profile of the metal-poor halo continues all the way out to at least 150 kpc (Gilbert et al. 2012; Ibata et al. 2014). Thus, our mass estimate is valid for the metal-poor ($[\text{Fe}/\text{H}] < -0.7$)

component of the halo. In particular, Ibata et al. (2014) find that $\sim 50\%$ of the halo stellar mass from 27–150 kpc to have $[\text{Fe}/\text{H}] < -0.6$ (see their Table 4). The fraction is comparable to the Brown et al. 2008 SFH result. Clearly, a large amount of the halo stellar mass is metal-rich, which could change the characteristics of the core radius for the total halo. Thus, while the metal-poor halo appears to have a consistent power-law index of ~ -2.5 from 3 to 150 kpc, the total halo is more complex, with multiple power-law indices, a larger core, and a larger mass.

If the large core radius of the total stellar halo is the result of the high-metallicity component, then one might expect the BHB/RGB ratio of the halo component to increase at smaller radii as the ratio of metal-poor stars to total stars increases. In Figure 6 we plot the expected ratio of metal-poor stars to total stars with galactocentric distance. We assume that the metal-poor component of the halo has a profile with a core radius of 3.5 kpc and a 2D power-law index of 2.7, and the metal-rich component has a core radius of 10.6 kpc and a 2D power-law index of 3.9. The result is that the metal-poor fraction has a minimum at 10–20 kpc, and a steep increase toward the galaxy center. These ratios are similar to those found by Gilbert et al. (2014), which were ~ 0.2 – 0.7 between 9 and 30 kpc, respectively. We are not able to match the spectroscopic ratios exactly because the difference in power-law index between the two components does not result in the fraction changing that steeply. We note that the spectroscopic sample in this radial range contains a significant amount of substructure (Gilbert et al. 2007), which may be causing the rapid change in the ratio of low-metallicity stars to total stars in those measurements. Therefore, we set the relative normalization between the two halo components so that in this radial range we roughly agree with the spectroscopic ratio of low metallicity stars to total stars.

If we assume a BHB/RGB fraction of ~ 5 , similar to low-metallicity globular clusters (Williams et al. 2012), for the metal-poor component, and a fraction of 0 for the metal-rich component, then we can convert the metal-poor fraction into an expectation for the BHB/RGB ratio of the halo as a whole with galactocentric distance. This relation is shown in Figure 6, and roughly follows the metallicity fraction.

Using these fractions along with the disk and bulge profiles from Dorman et al. (2013), we calculate the expected BHB/RGB ratios for the total population, which are plotted in Figure 5. This plot assumes that the metal-poor halo is the only component that has a significant BHB, and all components contribute to the RGB. The dashed, dotted, and gray lines assume a constant BHB/RGB halo fraction of 0.7 and the profiles of Courteau et al. (2011); Guhathakurta et al. (2005), and Dorman et al. (2013), respectively. The solid line assumes the BHB/RGB fraction of the halo component follows the relation shown in Figure 6, and the total profile follows that of the median fit from Dorman et al. (2013). Although still not a perfect match to the data, this relatively simple attempt to account for the changing metallicity of the halo moves the model prediction considerably closer to the data in the inner regions. Therefore, one way to reconcile the measurements is through an increasing metal poor fraction inside

⁹ measured without applying their masks to the substructure

of the Dorman et al. (2013) core radius.

Therefore, one explanation for the difference between the core radii of the BHB profile and the total halo profile could be that the metal-poor halo has a significantly smaller core than the metal-rich halo. Such a possibility may be testable in simulations, as many of the oldest, most metal-poor stars in the halo may actually form early and largely in the center of the dark matter halo. At the same time, if much of the metal-rich halo is formed later through accretion events, it could perhaps be hotter, resulting in a larger core. Our result can be compared to future simulations in this way.

3.2. The Stellar Halo Mass

If there is a significant amount of mass in the more metal-rich component of the halo which is not probed by the BHB stars, our previously-determined stellar halo mass of $2.1^{+1.7}_{-0.4} \times 10^9 M_{\odot}$ was not properly calibrated, as the profile was normalized to the total stellar surface brightness at 21 kpc ($\mu_V \sim 29$) from the photometry of Brown et al. (2008). Based on observations of globular clusters as well as stellar evolution theory, the BHB traces the metal-poor component of the stellar population. According to the star formation history (SFH) in Brown et al. (2008), about 50% of the stellar population has $[\text{Fe}/\text{H}] \lesssim -0.7$. If we assume a V -band stellar mass-to-light ratio of 2 for the metal-poor component (Bruzual & Charlot 2003; Chabrier 2003), and normalize by the fraction of metal-poor stars (0.5), our metal-poor halo stellar mass measurement is $1.5^{+1.1}_{-0.3} \times 10^9 M_{\odot}$. Since this only includes the metal-poor component, it is a lower-limit on the total stellar mass of the halo.

We can move beyond a lower limit if we assume the metal-rich component has a core radius of 10 kpc, as measured by Dorman et al. (2013) and the steep 2-D power-law slope of -3.72 measured by Ibata et al. (2014) for the unmasked metal-rich component. If we assume a V -band stellar mass-to-light ratio of 3 for the metal-rich component (Bruzual & Charlot 2003; Chabrier 2003) and normalize the metal-rich component to comprise the other half of the surface brightness at 21 kpc, then the mass of this component is $\sim 1.4 \times 10^9 M_{\odot}$. Adding this to the mass of the metal-poor component then yields a total of $\sim 3 \times 10^9 M_{\odot}$. This estimate is similar to our earlier estimate which did not properly account for the metal-rich component. This mass is about a factor of 2 lower than the estimates of Ibata et al. (2014). Their mass estimates do not assume a mass-to-light ratio, but instead fit the observed stars to correct to the full underlying populations.¹⁰ However, if we apply our assumed mass-to-light ratios of

2 and 3 directly to their measured V -band luminosities for the metal-rich and metal-poor components of the outer halo, the masses of these components are 2×10^8 and $4 \times 10^8 M_{\odot}$, respectively. Summing these values and extrapolating inward with an assumed core radius of 10 kpc yields an estimated total halo mass of $\sim 2 \times 10^9$. Thus, when the same assumptions are applied to both measurements, our halo stellar mass estimates are similar. However, ours is somewhat greater, largely due to the smaller core radius of the metal-poor component.

4. CONCLUSIONS

We have tested the predictions for the distribution of BHB stars from 30–40 arcmin (6–10 kpc) away from the center of M31 along the minor axis. The latest observations confirm the predictions based on a model where the BHB stars trace the metal-poor M31 stellar halo, and the metal-poor stellar halo has a structure that follows a power law with 2-D index $\alpha = 2.6^{+0.3}_{-0.2}$ inward to 3 kpc, then becomes significantly flatter near the galaxy center. This core-radius is significantly smaller than that measured for the total stellar halo. The BHB/RGB ratio we measure inside of 10 kpc suggests that the metal-poor halo component may become increasingly important inside of the total halo core radius of 10 kpc measured by Dorman et al. (2013). Therefore, not only does the slope of the stellar halo profile change with metallicity, the core radius appears to change with metallicity as well.

Combining this result with recent measurements of the total halo and metal-rich halo, suggests that the stellar halo mass calculated in (Williams et al. 2012) was likely underestimated because it did not properly account for the fact that the BHB stars were only probing the metal-poor component of the stellar halo. A more realistic calculation uses the metal-poor component, assuming a mass-to-light ratio of 2, to set a lower-limit on the stellar halo mass of $1.5^{+1.1}_{-0.3} \times 10^9 M_{\odot}$. If we estimate the mass of the metal-rich component using the Ibata et al. (2014) profile, assuming a metal-rich mass-to-light ratio of 3, and normalizing to the surface brightness at 21 kpc, then we can add this to the metal-poor component estimate to derive a total stellar mass of the M31 halo is $\sim 3 \times 10^9 M_{\odot}$. The significant differences between the metal-rich and metal-poor halo characteristics in M31 should be reflected in galaxy formation and evolution simulations.

Support for this work was provided by NASA through grant GO-12997 from the Space Telescope Science Institute, which is operated by the Association of Universities for Research in Astronomy, Inc., for NASA, under contract NAS 5-26555.

REFERENCES

- Bailin, J., Bell, E. F., Chappell, S. N., Radburn-Smith, D. J., & de Jong, R. S. 2011, *ApJ*, 736, 24
 Barker, M. K., Ferguson, A. M. N., Irwin, M., Arimoto, N., & Jablonka, P. 2009, *AJ*, 138, 1469
 Bell, E. F., et al. 2008, *ApJ*, 680, 295
 Brown, T. M., et al. 2008, *ApJ*, 685, L121
 Bruzual, G., & Charlot, S. 2003, *MNRAS*, 344, 1000
 Bullock, J. S., & Johnston, K. V. 2005, *ApJ*, 635, 931
 Bullock, J. S., Kravtsov, A. V., & Weinberg, D. H. 2001, *ApJ*, 548, 33
 Carignan, C., Chemin, L., Huchtmeier, W. K., & Lockman, F. J. 2006, *ApJ*, 641, L109
 Chabrier, G. 2003, *PASP*, 115, 763
 Cooper, A. P., et al. 2010, *MNRAS*, 406, 744
 Courteau, S., Widrow, L. M., McDonald, M., Guhathakurta, P., Gilbert, K. M., Zhu, Y., Beaton, R. L., & Majewski, S. R. 2011, *ApJ*, 739, 20
 Dalcanton, J. J., et al. 2012, *ApJS*, 200, 18
 Deason, A. J., Belokurov, V., Evans, N. W., & Johnston, K. V. 2013, *ApJ*, 763, 113

¹⁰ The luminosities are measurements within their selection function.

- Dolphin, A. E. 2000, *PASP*, 112, 1383
- Dorman, C. E., et al. 2013, *ApJ*, 779, 103
- Gilbert, K. M., et al. 2007, *ApJ*, 668, 245
- Gilbert, K. M., Font, A. S., Johnston, K. V., & Guhathakurta, P. 2009, *ApJ*, 701, 776
- Gilbert, K. M., et al. 2012, *ApJ*, 760, 76
- Gilbert, K. M., et al. 2014, *ArXiv e-prints*
- Greggio, L., Rejkuba, M., Gonzalez, O. A., Arnaboldi, M., Iodice, E., Irwin, M., Neeser, M. J., & Emerson, J. 2014, *A&A*, 562, A73
- Guhathakurta, P., Ostheimer, J. C., Gilbert, K. M., Rich, R. M., Majewski, S. R., Kalirai, J. S., Reitzel, D. B., & Patterson, R. J. 2005, *ArXiv: astro-ph/0502366*
- Ibata, R., Irwin, M., Lewis, G., Ferguson, A. M. N., & Tanvir, N. 2001, *Nature*, 412, 49
- Ibata, R. A., et al. 2014, *ApJ*, 780, 128
- Johnston, K. V., Bullock, J. S., Sharma, S., Font, A., Robertson, B. E., & Leitner, S. N. 2008, *ApJ*, 689, 936
- Jurić, M., et al. 2008, *ApJ*, 673, 864
- Kalirai, J. S., et al. 2006a, *ApJ*, 648, 389
- Kalirai, J. S., et al. 2006b, *ApJ*, 648, 389
- Koch, A., et al. 2008, *ApJ*, 689, 958
- McConnachie, A. W., et al. 2009, *Nature*, 461, 66
- Pillepich, A., et al. 2014, *ArXiv e-prints*
- Sesar, B., Jurić, M., & Ivezić, Ž. 2011, *ApJ*, 731, 4
- Stanek, K. Z., & Garnavich, P. M. 1998, *ApJ*, 503, L131
- Tanaka, M., Chiba, M., Komiyama, Y., Guhathakurta, P., Kalirai, J. S., & Iye, M. 2010, *ApJ*, 708, 1168
- Williams, B. F., et al. 2012, *ApJ*, 759, 46
- Zolotov, A., Willman, B., Brooks, A. M., Governat o, F., Brook, C. B., Hogg, D. W., Quinn, T., & Stinson, G. 2009, *ApJ*, 702, 1058

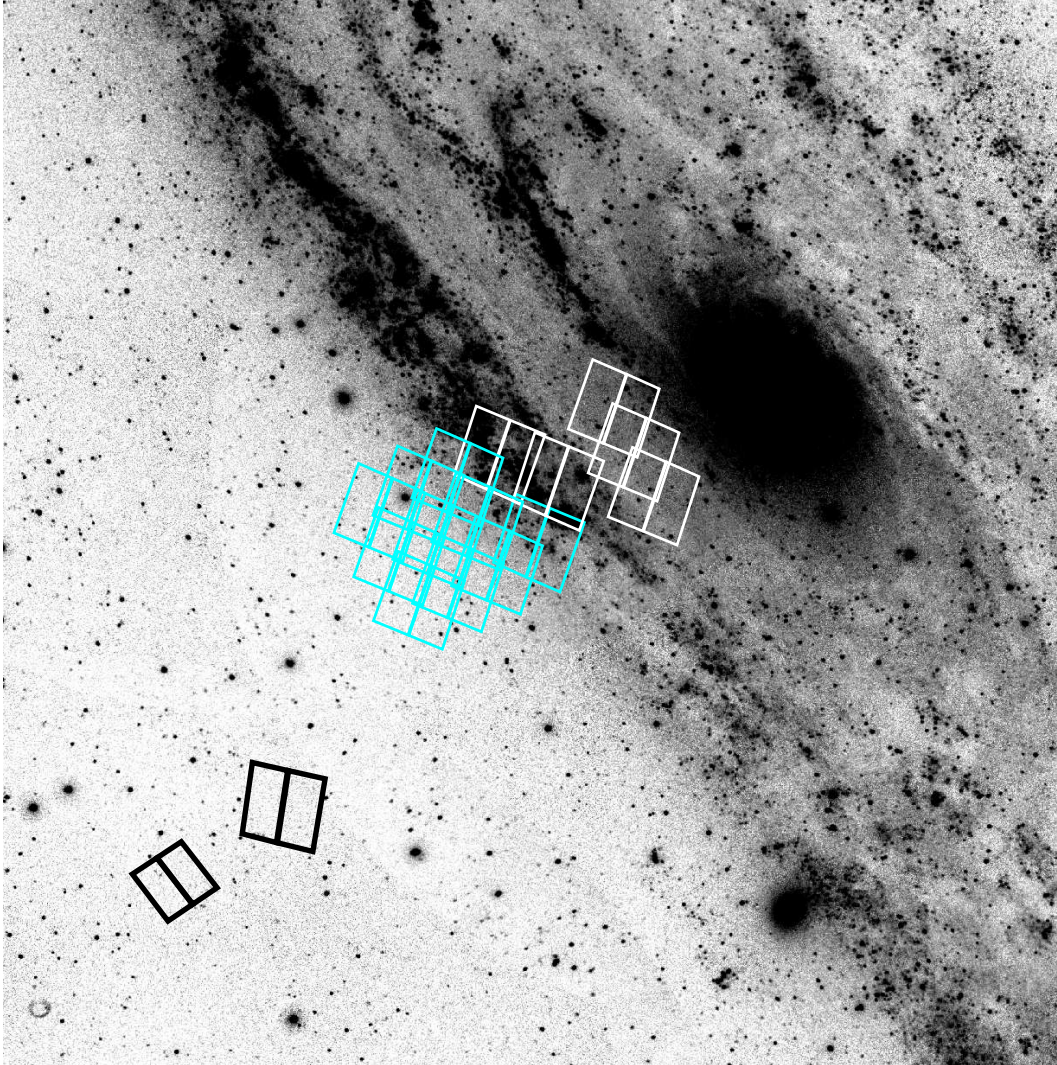


FIG. 1.— Black rectangles mark the location of our new ACS and UVIS fields along the minor axis of M31. Cyan rectangles mark the fields from Williams et al. (2012) that resulted in a BHB density measurement. While rectangles mark the fields from Williams et al. (2012) that allowed BHB density upper limit measurements.

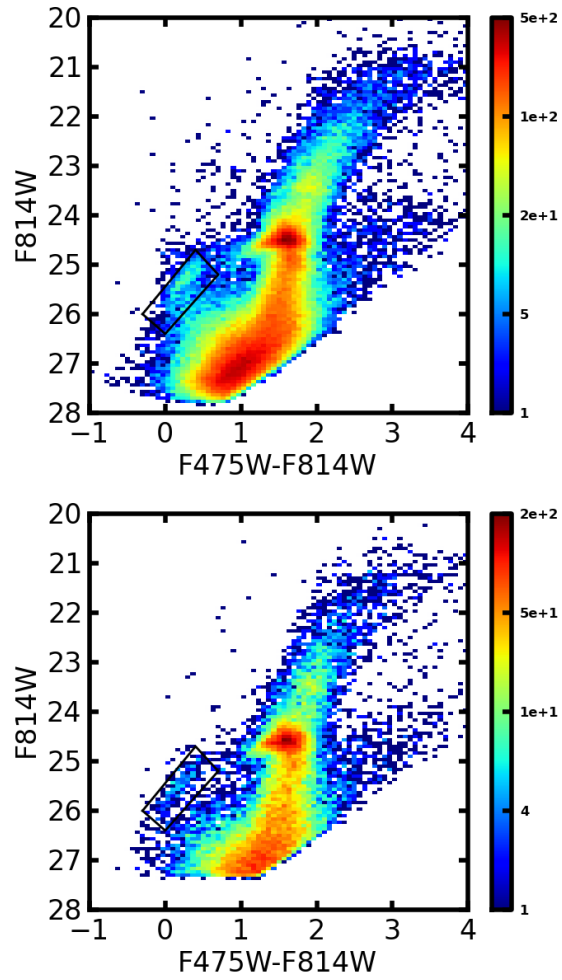


FIG. 2.— Color-magnitude diagrams (CMDs) from the ACS (*top*) and UVIS (*bottom*) imaging data. The BHB is outlined. The UVIS field has significantly fewer stars because it is smaller and farther out.

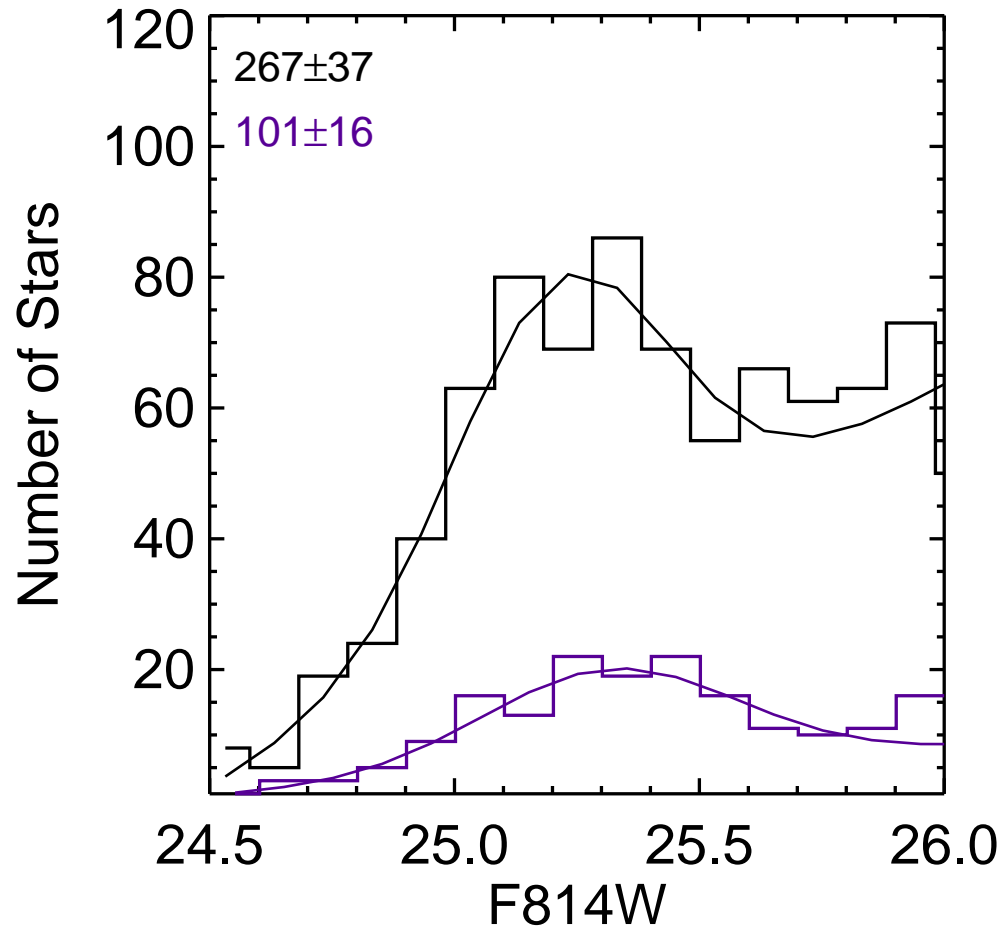


FIG. 3.— Fits to the luminosity function near the BHB in our two new HST fields. A clear peak is detected, and the number of stars in the feature is given in the upper-left for each field.

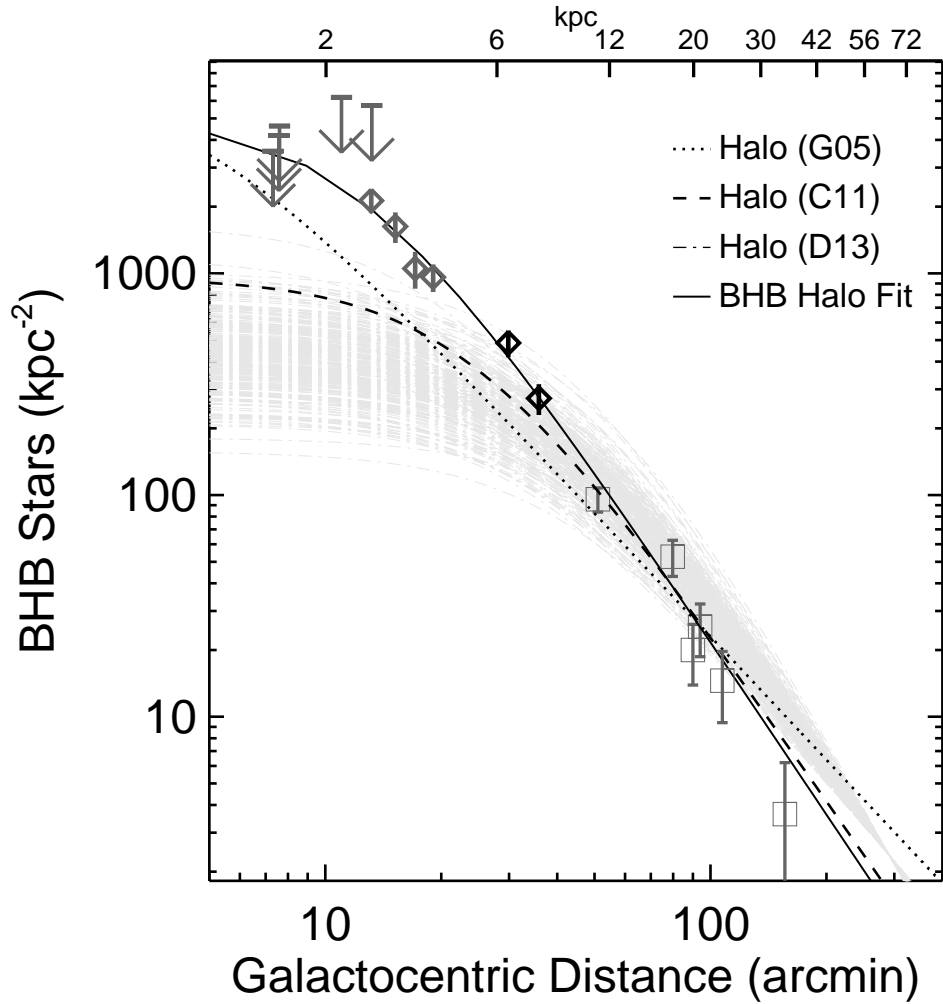


FIG. 4.— The number density of BHB stars measured for these fields (black data points at $30'$ and $36'$) overplotted on the radial distribution found in Williams et al. (gray points; 2012). Solid, dashed, and dotted lines mark the halo fits from Williams et al. (2012), from Courteau et al. (2011), and Guhathakurta et al. (2005), respectively. Light gray dot-dashed lines mark a random draw of 256 MCMC results from Dorman et al. (2013). The new data in the previously-unobserved region agrees with the model profile determined assuming that the BHB traces the low metallicity component of the stellar halo.

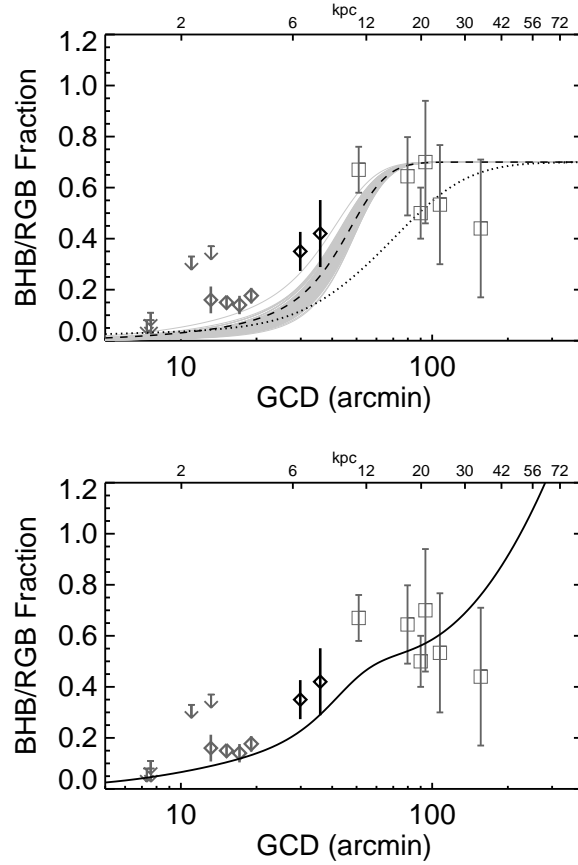


FIG. 5.— The BHB/RGB ratio as a function of radius. Gray points are from Williams et al. (2012). Black points are from the new observations at $30'$ and $36'$. *Top*: Dashed, and dotted lines assume a constant BHB/RGB ratio of the pure halo of 0.7 (Williams et al. 2012) and the halo fractions as a function of radius from Courteau et al. (2011), and Guhathakurta et al. (2005), respectively. Gray lines also assume a constant BHB/RGB ratio of the pure halo of 0.7 but the halo fractions come from 256 trials from the Dorman et al. (2013) analysis. The strong transition between dominant components was predicted to occur in the previously-unobserved region from $20'$ to $60'$, and indeed, the new observations (at $30'$ and $36'$) follow the predicted sharp transition. *Bottom*: To match the sharp transition in BHB/RGB ratio, as well as the inner data points, requires an increase in the fraction of metal-poor halo stars inside of 10 kpc, as shown with the black solid line. This line is the result of extrapolating of the metal-rich halo profile of Ibata et al. (2014) inward, adopting the stellar halo core radius measured by Dorman et al. (2013) for the metal-rich component core radius, and adopting the BHB core radius and power-law index for the metal-poor halo component. Even this two-component halo model does not fully match the data; however, it is a significant improvement over any single-metallicity option, assuming previously-measured decomposition parameters.

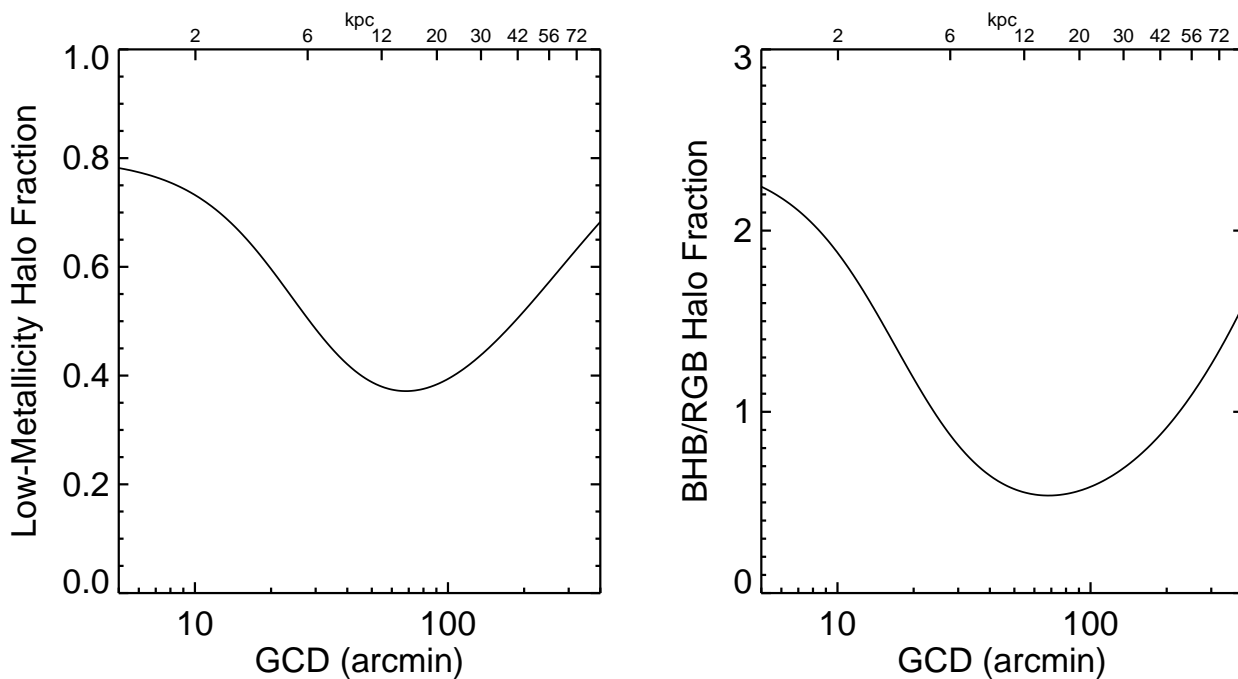


FIG. 6.— *Left*: The fraction of metal-poor ($[\text{Fe}/\text{H}] < -0.7$) halo stars as a function of galactocentric distance predicted by extrapolating the Ibata et al. (2014) metal-rich halo profile, adopting the Dorman et al. (2013) core radius for the metal-rich component, and adopting the BHB profile for the metal-poor component. Because of the smaller core radius of the metal-poor component, the metal-poor fraction recovers inside of the metal-rich core radius. *Right*: The predicted BHB/RGB ratio of the halo alone as a function of galactocentric distance, assuming the metal-poor component has a ratio of 5, comparable to metal-poor globular clusters (Williams et al. 2012). The high value in the inner galaxy is again due to the smaller core radius of the metal-poor component.